ABDOMINAL IMAGING

I J Radiol. 2024 April; 21(2): e143996. https://doi.org/10.5812/iranjradiol-143996.

Published online: 2024 September 29. **Research Article**

Shear Wave Elastography in Evaluating the Efficacy of Liver Microwave Ablation: An Experimental Study

Dandan Xu [1], Chao Tian [2], Shan Wei [1,*]

[1] Haikou Affiliated Hospital, School of Medicine, Central South University Xiangya, Hu Nan Sheng, China
[2] Shenzhen Baoan Women's and Children's Hospital, Shenzhen, China

[*] *Corresponding author:* Haikou Affiliated Hospital, School of Medicine, Central South University Xiangya, Hu Nan Sheng, China. Email: shanweishan286@163.com

Received 2024 January 31; **Revised** 2024 August 12; **Accepted** 2024 August 14.

Abstract

Background: The effect of microwave ablation on small hepatocellular carcinoma is not significantly different from that of surgical resection. Accurate assessment of the ablation effect is crucial for ensuring the safety and effectiveness of hyperthermia.

Objectives: This study aimed to explore the feasibility and accuracy of supersonic shear wave elastography (SWE) in quantitatively evaluating the microwave ablation margin of the liver.

Materials and Methods: Three surgeons were each randomly assigned 4 Wuzhishan miniature pigs (WZSPs) to perform 12 ablation procedures at an ablation power of 40 W. Based on the ablation time, the lesions were divided into 15, 30, and 60-second groups. Immediately after ablation, SWE and modulus measurements were performed 5 times for each ablation lesion. The SWE data were expressed as mean ± standard deviation. Within-group and between-group comparisons were made using repeated measures analysis of variance.

Results: A total of 144 effective ablations and 131 effective pathological results were obtained. Within the same ablation time, the elastic modulus increased in the surrounding normal tissue, ablation margin, and ablation center regions in a stepwise manner ($P < 0.01$). However, in the ablation center region, the elastic modulus decreased in a stepwise manner with the shortening of ablation time [60 s (97.16 ± 14.58 kPa) > 30 s (77.84 ± 9.64 kPa) > 15 s (38.92 ± 3.12 kPa)], with statistically significant differences ($F = 2,131.832$, $P < 0.01$). The elastic modulus of the ablation margin region at different ablation times remained between 22.68 - 23.56 kPa.

Conclusion: The elastic modulus range in the ablation margin region after microwave ablation is relatively fixed. Shear wave elastography aids in the quantitative evaluation of the ablation margin region of the liver and has high practical value in monitoring and evaluating ultrasound ablation.

Keywords: Elastography, Shear Wave, Microwave Ablation, Ablation Boundary, Elastic Modulus

1. Background

According to the 2020 Global Cancer Survey, liver cancer is the sixth most common cancer and the third leading cause of cancer-related mortality worldwide (1). Current therapeutic methods for liver cancer include chemoradiotherapy, targeted immunotherapy, and surgical resection. However, challenges such as postoperative recurrence, drug resistance, and poor long-term efficacy persist (2). Personalized comprehensive treatment has shown more obvious advantages over traditional surgical methods and has become the main focus of liver cancer treatment development (3).

Microwave ablation is widely used in the minimally invasive treatment of liver cancer due to its high penetrability and controllable ablation range, serving as an alternative or supplementary approach to some liver cancer surgeries (4). Additionally, it is commonly used for the palliative and non-curative treatment of liver tumors, characterized by less trauma, high applicability, and ease of operation (5). Because of the technical limitations of traditional microwave ablation, its range is primarily estimated using two-dimensional (2D)

grayscale images and the surgeon's experience, which results in high subjectivity and low accuracy (6).

In recent years, with the ongoing advancement of supersonic shear wave technology in medical ultrasound, supersonic shear wave elastography (SWE) has become a viable option (7). Shear wave elastography, also known as ultrasound elastography, can quantitatively evaluate the hardness of various tissues, thereby assisting radiologists in distinguishing tumor boundaries and defining tumor properties. Studies have revealed that SWE has significant advantages in the diagnosis and evaluation of solid tumors (8, 9). Microwave ablation is widely applied as a minimally invasive treatment for liver cancer due to its relatively effective penetration and conformal ablation. Accurately evaluating the completeness of ablation is crucial for ensuring safety and improving efficacy (10). Research has shown that elastography has practical value and broad prospects in the monitoring and evaluation of microwave ablation (11).

2. Objectives

Using Wuzhishan miniature pigs (WZSPs) as a large animal model, the present study explores the feasibility and accuracy of SWE in quantitatively evaluating the microwave ablation margin of the liver. By measuring the elastic modulus of the ablation margin, the critical elastic modulus for the irreversible necrosis of margin cells is predicted at the cellular level in combination with the hematoxylin and eosin (H&E) and nicotinamide adenine dinucleotide hydrate (NADH) diaphorase staining results of the pathological specimens.

3. Materials and Methods

3.1. Animals Used in the Experiment and Primary Materials

According to the resource equation (12), the sample size required for this study was at least 11. Therefore, 12 healthy male WZSPs were included. The WZSPs had a body weight of 15 ± 0.5 kg and were approximately 5 months old; they were purchased from the Institute of Animal Science and Veterinary Medicine, Hainan Academy of Agricultural Sciences, China. The WZSP is a native breed of China, known for its naturally small size, genetic stability, tolerance to coarse fodder, and strong resistance to reversion. In this study, the WZSPs were kept under experimental conditions in metal-fenced enclosures with concrete floors. Each enclosure measured 30 m^2 in size and 1.6 m in height. The temperature range of the pig house was maintained at 18°C - 25°C, with relative humidity between 40% and 60%. The WZSPs were fed twice a day, supplemented with a small amount of green vegetables or high-quality grass. The daily feed quantity was calculated according to the pig's weight and was generally 2% - 3% of its body weight.

The pigs used in the experiment were castrated after they were 14 days old. The WZSPs were placed with their hind legs on a smooth fence, and the surgical site was disinfected with alcohol or 2% iodine (Shandong Keyue Medical Technology Co. Ltd., China). Lidocaine anesthetic (Shanghai Pujin Linzhou Pharmaceutical Co. Ltd., China) was injected subcutaneously through the groin into each testicle (0.5 mL per site) and each spermatic cord (0.5 mL per site). A 1-cm incision was made in the scrotum of each testicle, and the testicle was extracted from the scrotum. An antibacterial ointment or spray was applied to the wound surface after suturing. The castrated pigs were then placed in a birthing bed under a thermal lamp to recover slowly. Treatment of the animals adhered to the GB/T 35892-2018 Guidelines for the Ethical Review of Laboratory Animal Welfare.

The reagents, nitroblue tetrazolium (NBT), oxidized coenzyme I β-NADH, and phenazine methosulfate (PMS), were all purchased from Sigma (USA). Additionally, an EC0 - 100C ultrasound-guided microwave tissue coagulation device for solid tumors, an Aixplorer ultrasound diagnostic instrument (SuperSonic Imagine, France), a SCI5-4 linear-array probe (frequency of 4 - 15 MHz; SuperSonic Imagine, France), and a 2700-Frigocut cryomacrotome (Reichert–Jung, China) were used in this study.

3.2. Experiment Methods

3.2.1. Preoperative Preparation

Before the experiment, the WZSPs were fasted for 2 days and prohibited from drinking water for 1 day. They were then sent to the cleaning room to be cleaned and dried. Subsequently, they were intraperitoneally injected with 3% pentobarbital sodium (Beijing Jiehui Biology, China) at a dose of 1 mL/kg. After being anesthetized, they were fixed to the operating table, with an indwelling needle inserted into the ear vein for

an intravenous drip of 3% pentobarbital sodium (Beijing Jiehui Biology, China) at 0.2 mL/min for anesthesia maintenance. The vital signs of the pigs were monitored intraoperatively and, when necessary, a subcutaneous injection of 0.15 mg/mL xylazine hydrochloride (Jilin Huamu Animal Health Products Co. LTD, China) was administered to deepen anesthesia (13). Appropriate humane care was provided in accordance with the Guidelines for the Ethical Review of Laboratory Animal Welfare, and every effort was made to minimize their pain and suffering.

3.2.2. Microwave Ablation Under Direct Vision

Three surgeons conducted the experiment, with each surgeon randomly assigned 4 WZSPs to perform 12 ablation procedures. The abdominal skin was shaved and disinfected, and an L-shaped incision was made in the mid-abdomen to expose the liver. The liver of the WZSP was divided into 5 lobes: The left outer lobe, left inner lobe, right inner lobe, right outer lobe, and the middle lobe posteromedial to the right inner lobe. The middle lobe was further divided at the hepatic hilum into the dorsal caudate lobe and ventral quadrate lobe. Microwave ablation mainly targeted the 4 relatively thick lobes, as well as the middle lobe.

Under the guidance of 2D ultrasound, a microwave ablation needle was inserted into the hepatic lobe, aiming for a location far from the hepatic surface, with relatively uniform hepatic tissue and a sparse intrahepatic duct system. The cooling circulation pathway was then activated, and the microwave ablation electrode was triggered, using an ablation power of 40 W. The 4 hepatic lobes were ablated for 15, 30, and 60 seconds.

3.2.3. Shear Wave Elastography

Two radiologists, who were blinded to the ablation process, performed 2D ultrasound and SWE on the ablation lesions. Immediately after ablation, a 2D ultrasound was conducted to scan the ablation lesion in multiple sections. When the section with the largest ablation lesion was identified, the size of the lesion was measured. Subsequently, under the guidance of a stabilized ultrasound probe, the SWE program was run in dual-amplitude mode to maintain section consistency, with a color-coding range of 0 - 180 kPa.

The SWE sampling frame (a 4 × 3 cm rectangle) covered the entire lesion and the surrounding hepatic parenchyma. With 5 - 6 frames of stable elastography, the SWE was converted to a color spectrum based on different tissue hardness. Simultaneously, the SWE measurement program (Q-BOXTM) was used to measure the elastic modulus of the region of interest within the entire lesion, recording and storing the maximum, minimum, and mean elasticity, as well as the discrepancy, using kPa units. The examination was considered successful when the color remained stable and occupied at least 2/3 of the sampling frame, with no color misjudgment caused by excessive manipulation in front of the section, no noise interference behind the section, and relatively consistent changes in elastic images. Shear wave elastography was performed 5 times for each ablation lesion, and elastic modulus measurements were taken after each SWE.

3.2.4. Enzyme Histochemical Staining

A pathologist prepared pathology sections of the ablation foci for observation. After all measurements were taken, a total liver resection was performed. Postoperatively, the experimental animals were euthanized using an anesthesia overdose. The liver tissues with ablation lesions were collected as specimens, with 5 mm of surrounding normal tissue retained. Consistency between the anatomical and SWE sections was ensured under 2D ultrasound monitoring. Each ablation lesion was evenly cut open along the maximum section perpendicular to the microwave needle track. Each tissue with an ablation lesion was divided into 2 parts: One part was fixed with formaldehyde and stained with H&E, while the other part was quickly frozen in liquid nitrogen and embedded in an optimal cutting temperature (OCT) compound as a frozen section, which was then subjected to NADH diaphorase histochemical staining. Two flat and non-folded paraffin sections and frozen sections were selected from each specimen.

The procedure was conducted as follows: (1) preparation of the incubation buffer: 100 mg of NBT, 50 mg of NAD, 80 mL of phosphate buffer, 10 mg of PMS, and 20 mL of a 4% sodium lactate solution were added successively and stirred multiple times until fully dissolved. After filtering through coarse filter paper, the incubation buffer was obtained and stored in a refrigerator at 4°C in the dark; (2) preparation of the

frozen section: The slicer temperature was preset (temperature: -19 °C; temperature in the cold chamber: -6 °C). The liquid nitrogen-preserved specimen was removed, edge-trimmed on a frozen slicer with 5 mm of surrounding normal tissue retained, embedded in OCT, and sliced into sections with a thickness of 4 μm. The flat and non-folded frozen section was gently attached to a glass slide and kept at room temperature after rinsing with double-distilled water; (3) section staining: The sections were neatly placed into the incubation box, into which the incubation buffer was slowly poured to immerse the glass slides. After immersion for 30 minutes, the glass slides were removed one by one using tweezers, gently rinsed with double-distilled water for 10 minutes, dried in a constant-temperature box, and sealed with the prepared glycerine jelly. Phosphate-buffered saline was used instead of sodium lactate as a negative control. The distance between the ablation margin and the ablation center (needle track) was observed and measured under a microscope.

3.3. Statistical Analysis

The experimental data were analyzed using SPSS 22.0 software (IBM Corp. Released 2013. IBM SPSS Statistics for Windows, Version 22.0. Armonk, NY: IBM Corp.). The SWE data conforming to a normal distribution were described as mean ± standard deviation. Within-group and between-group comparisons were performed using repeated measures analysis of variance (ANOVA). Trend analysis was used to test the linear change (decrease/increase) in the index post-ablation. A P-value of < 0.05 was considered statistically significant.

4. Results

4.1. Microwave Ablation Data

In this experiment, a total of 144 effective ablations and 720 effective SWE measurements were performed, and 131 effective pathological results were obtained. The specific procedures for microwave ablation for 15, 30, and 60 seconds at an ablation power of 40 W are summarized in Table 1.

4.2. Analysis of Pathological Results

4.2.1. Naked-Eye Observation

The ablation lesion was divided into four regions: Needle tract, needle tract periphery, ablation margin, and surrounding normal tissue. The needle tract region and needle tract periphery together constituted the ablation center region. Under H&E staining, with relatively blurred region boundaries, the ablation lesion was divided into three regions: The ablation center (orange arrow), ablation margin (blue arrow), and surrounding normal tissue (green arrow). The needle tract region could be observed within the ablation center region. Under NADH diaphorase histochemical staining, three regions were clearly identified in the 30- and 60-second ablation lesions.

4.2.2. Microscope Observation

The ablation center (necrotic) region was mainly characterized by coagulation necrosis, with cells losing their original activity and appearing as a red stripe. In the ablation margin region, due to the coexistence of necrosis and hemi necrosis, both red stripe-shaped tissue and a small amount of purple granule-like tissue were observed. The surrounding normal tissue region primarily manifested as purple granule-like tissue.

4.3. Shear Wave Elastography Measurement Results

4.3.1. Post-ablation Shear Wave Elastography Images

The post-ablation elastography images clearly showed that the ablation lesion was divided into three regions. The ablation center region appeared red or yellow, the ablation margin region appeared cyan, and the surrounding normal tissue region appeared dark blue.

4.3.2. Comparison of Post-ablation Shear Wave Elastography Measurement Parameters

The results of repeated measures ANOVA showed that both the main effect of time and the main effect of group were statistically significant ($F = 716.000$, $P < 0.01$; $F = 15{,}302.863$, $P < 0.01$). There was also a significant interaction between time and group ($F = 1{,}432.000$, $P < 0.01$) (Table 2).

A comparison of the elastic modulus of the ablation margin region (22.44 ± 7.17 vs. 23.75 ± 5.84 vs. 22.94 ± 4.91, $P = 0.058$) and the surrounding normal tissue region (7.49 ± 1.83 vs. 7.85 ± 2.16 vs. 7.81 ± 2.04, $P = 0.105$) after ablation for 15, 30, and 60 seconds at an ablation power

Table 1. Data on Microwave Ablation of Porcine Liver Under Different Ablation Time

Ablation time (s)	Effective ablation lesion (n)	Effective SWE measurement (times)	Effective pathological result (n)
15	48	240	45
30	48	240	42
60	48	240	44
Total	144	720	131

Abbreviation: SWE, shear wave elastography.

Table 2. The Repeated Measures Analysis of Variance Results

Factor	F	P-value
Region	15302.863	< 0.01
Time	716.000	< 0.01
Region × time	1432 .000	< 0.01

of 40 W revealed no statistically significant differences. However, in the ablation center region, the elastic modulus decreased gradually as the ablation time was shortened, with statistically significant differences (38.92 ± 3.14 vs. 77.84 ± 9.58 vs. 116.37 ± 18.41, $P < 0.01$).

By analyzing the three ablation time groups separately, it was revealed that the pattern of elastic modulus variation was as follows: Ablation center region > ablation margin region > normal tissue region, with statistically significant differences ($P < 0.01$; Table 3 and Figure 1). Notably, in the SWE measurement after ablation for 15 seconds at an ablation power of 40 W, although a statistically significant difference was observed in the elastic modulus between the ablation center and ablation margin regions, the specific values overlapped, and the difference was not as pronounced as in the measurements after ablation for 30 and 60 seconds. According to the results of our experiment, the average elastic modulus of the ablation margin in the samples remained at 23.05 ± 6.06 kPa.

5. Discussion

Shear wave elastography is an ultrasound imaging technology developed in recent years that directly measures the hardness of biological tissue using ultrasound. Both domestic and international research have demonstrated that elastography has high practical value and broad application prospects in monitoring and evaluating ultrasound ablation (14). Accurately evaluating the ablation effect is crucial for ensuring the safety and improving the efficacy of ablation. A study by Zhu and Zhu (10) indicated that ultrasound elastography can preliminarily reflect the degree of coagulative necrosis in liver lesions. Luo et al. (15) demonstrated that elastography clearly displays the margins of radiofrequency ablation lesions and is expected to become an effective method for evaluating radiofrequency ablation lesions. The preliminary research in this experiment also indicates the feasibility of elastography in evaluating the range of ablation lesions.

In the present study, using WZSPs as experimental animals, microwave ablation lesions were created in the four hepatic lobes by ablating for 15, 30, and 60 seconds at an ablation power of 40 W. Immediately after surgery, the elasticity images of the ablation lesions were collected, and the elasticities were calculated. Additionally, the feasibility and accuracy of SWE in the quantitative evaluation of microwave ablation margins of the liver were explored. Protein denaturation occurs in liver tissue through an effective thermal field, which leads to a significant increase in hardness. During ablation, the elastic modulus in this region increases significantly and is positively correlated with ablation time, and carbonization may even occur.

The peripheral bleeding zone, also known as the ablation margin region, is a narrow band-like area of bleeding with some inflammatory cell infiltration. Because this study used immediate pathological sections after ablation, inflammatory cell infiltration was not significant. The pathology results revealed that necrotic and heminecrotic tissue coexisted in this

Table 3. Elastic Modulus of Porcine Liver at Different Ablation Times and Regions (kPa) [a-h]

Ablation time (s)	Effective SWE measurement (times)	Normal tissue region	Ablation margin region	Ablation center region	F	P-value
15	240	7.49 ± 1.83	22.44 ± 7.17 [c]	38.92 ± 3.14 [d]	2752.470	< 0.01
30	240	7.85 ± 2.16	23.75 ± 5.84 [e]	77.84 ± 9.58 [a,f]	7415.498	< 0.01
60	240	7.81 ± 2.04	22.94 ± 4.91 [g]	116.37 ± 18.41 [b,h]	6780.600	< 0.01
F-value		2.260	2.853	2451.015		
P-value		0.105	0.058	< 0.01		

Abbreviation: SWE, shear wave elastography.

[a] Compared with the 15-s ablation group, difference is statistically significant ($t = 61.235$, $P < 0.05$).

[b] Compared with the 15-s ablation group and the 30-s ablation group, difference is statistically significant ($t = 62.467, 17.127$, $P < 0.05$).

[c] Compared with the normal tissue region in the 15-s ablation group, difference is statistically significant ($t = 15.110$, $P < 0.05$).

[d] Compared with the normal tissue region and ablation margin region in the 15-s ablation group, difference is statistically significant ($t = 31.411, 16.300$, $P < 0.05$).

[e] Compared with the normal tissue region in the 30-s ablation group, difference is statistically significant ($t = 15.984$, $P < 0.05$).

[f] Compared with the normal tissue region and ablation margin region in the 30-s ablation group, difference is statistically significant ($t = 69.983, 53.999$, $P < 0.05$).

[g] Compared with the normal tissue region in the 60-s ablation group, difference is statistically significant ($t = 15.138$, $P < 0.05$).

[h] Compared with the normal tissue region and ablation margin region in the 60-s ablation group, difference is statistically significant ($t = 89.361, 74.224$, $P < 0.05$).

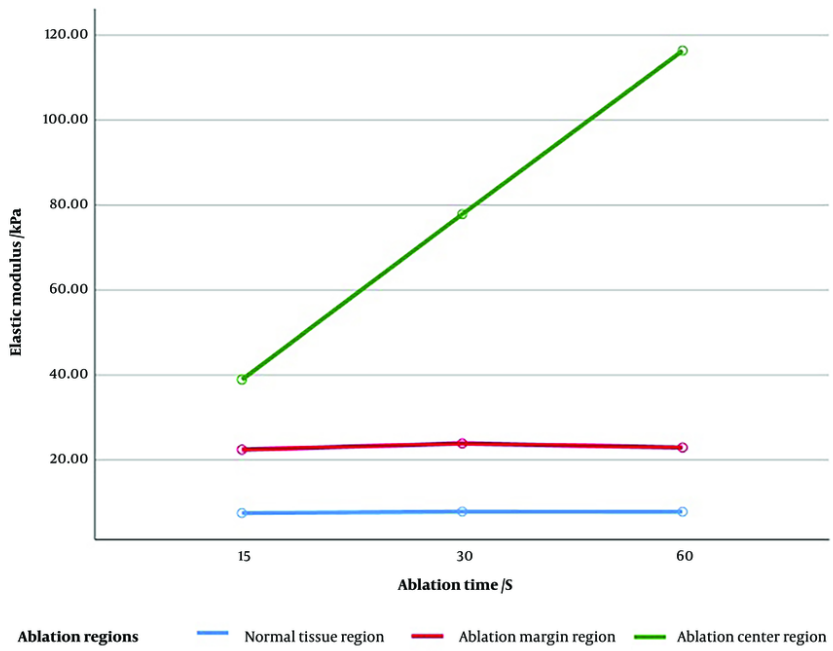

Figure 1. Elastic modulus of porcine liver at different ablation times and regions (kPa)

(heminecrotic) region. The position of the ablation margin region is not fixed. Generally, as the ablation time increases, the margin region moves away from the ablation center (16), but its elastic modulus is relatively constant. The SWE image immediately post-ablation displayed the near-field boundary and the vertical and anteroposterior boundaries of the ablated area through color differences, which supports the notion that elastography is less affected by gas (17).

Elastography is color-coded based on the differences in tissue hardness after ablation, forming three regions centered on the electrode. The ablation center region appeared red or yellow, the ablation margin region appeared cyan, and the surrounding normal tissue region appeared dark blue. Additionally, the distribution of Young's modulus in these three regions was observed and measured, revealing no statistically significant difference in the elastic modulus between the surrounding normal tissue region and the ablation margin region. This result indicates that for a large or deeply ablated area, SWE measurements may underestimate the vertical diameter. However, in the ablation center region, the elastic modulus decreased progressively with shorter ablation times, showing statistically significant differences.

By analyzing the three ablation time groups separately, it was found that the elastic modulus variation pattern exhibited a regularly decreasing trend centered on the electrode. This indicates that SWE can preliminarily reflect the distribution of tissue hardness immediately after ablation, which is consistent with the conclusions of multiple studies (18-20). Luo et al. identified some remaining overestimates in SWE values immediately post-ablation, with most of the SWE values stabilizing at 5 minutes (21). Therefore, SWE measurements should not be performed too early after ablation. Crocetti et al. determined that SWE was not able to reliably capture changes in stiffness within, at the border of, and outside the necrotic zone in an ex vivo liver model (20).

Zhou et al. (22) reported on 18 patients with uterine myoma who underwent microwave ablation and compared the SWE measurement results with those of contrast-enhanced ultrasound and enhanced magnetic resonance imaging (MRI). The outcomes revealed no statistically significant difference between the results of elastography and those of contrast-enhanced ultrasound or MRI, suggesting that SWE is not inferior to imaging methods such as MRI in evaluating the microwave ablation range in uterine myoma. Tian et al. (23) reported the elastic modulus of 57 patients with liver tumors after radiofrequency ablation at 30 minutes, 1 day, and 1 month, identifying no statistically significant differences and demonstrating that SWE can quantitatively analyze the elastic modulus changes in liver tumors before and after radiofrequency ablation. Kang et al. (24) used acoustic radiation force impulse to demonstrate the correlation between shear wave echo velocity and the degree of ablation-induced injury, providing a theoretical basis for the use of elastography in evaluating ablation-induced injury. Moreover, according to the research results of Huang et al. (25) and Zhang et al. (26), the elastic modulus is positively correlated with the degree of tissue damage during microwave ablation.

5.1. Limitations

The effect of microwave ablation on living tissue differs from that on isolated tissue. Due to the influence of blood flow in living tissue, the ablation volume in living tissue is smaller than that in isolated tissue under the same microwave dose. Moreover, the volume of living liver masses is relatively large, and the internal echo is uneven, which causes interference with SWE imaging. Therefore, this paper only discusses the general pattern of strain elasticity in evaluating the value of ablation lesions through in vitro tissue. To further apply our findings to clinical practice, more comprehensive live animal experiments and clinical case studies are needed.

Challenging factors in applying our results to the evaluation of human ablation lesions remain, including the presence of ribs, abdominal wall thickness, breathing, and heartbeat. Thus, the use of strain elastic imaging to determine the scope of ablation in vivo requires further study. Additionally, in this study, the different areas around the microwave electrode were mainly defined based on pathological findings, such as the percentage of cell necrosis. However, the consistency of these pathological areas with the SWE map was not determined in this study and should be further explored in future research. Finally, the study's sample size is limited, with only a small number of ablation foci observed and measured, and the display and evaluation capabilities of 2D ultrasound and SWE imaging under the condition of further enlargement of ablation foci were not assessed. Further research is required to increase the ablation power and time.

In conclusion, the range of the elastic modulus in the ablation margin region is relatively fixed, and the elastic modulus in ablation lesions presents a stepped concentric distribution, providing a basis for the use of SWE in the quantitative evaluation of the ablation margin region. By tracking and delineating the ablation margin, SWE can assist operators in further clarifying

the effective killing range of microwave ablation. This allows for more precise control of the distribution of completely necrotic and heminecrotic regions and better protection of key peripheral organs and tissues while ensuring the maximum effective destruction of tumor tissue.

Acknowledgements

All data generated or analyzed during this study are included in this published article.

Footnotes

Authors' Contribution: Study conception and design: Xu DD, Tian C, Data collection: Wei S, Data analysis and interpretation: All authors, Drafting of the article: All authors. Critical revision of the article: All authors.

Conflict of Interests Statement: The authors declared no conflict of interests.

Data Availability: All data generated or analyzed during this study are included in this published article.

Ethical Approval: This study is approved under the ethical approval code of the Animal Experimentation Ethics Committee of Haikou Affiliated Hospital of Central South University Xiangya School of Medicine (2015KYLS020) in compliance with national or institutional guidelines for the care and use of animals.

Funding/Support: This work was supported by 2016 Hainan Provincial Natural Science Foundation Project: "Experimental study on immediate evaluation of liver microwave ablation lesion boundaries using ultra-high-speed shear wave elastography" (No. 20168311).

References

1. Maomao C, He L, Dianqin S, Siyi H, Xinxin Y, Fan Y, et al. Current cancer burden in China: epidemiology, etiology, and prevention. *Cancer Biol Med*. 2022;**19**(8):1121-38. [PubMed ID: 36069534]. [PubMed Central ID: PMC9425189]. https://doi.org/10.20892/j.issn.2095-3941.2022.0231.
2. Anwanwan D, Singh SK, Singh S, Saikam V, Singh R. Challenges in liver cancer and possible treatment approaches. *Biochim Biophys Acta Rev Cancer*. 2020;**1873**(1):188314. [PubMed ID: 31682895]. [PubMed Central ID: PMC6981221]. https://doi.org/10.1016/j.bbcan.2019.188314.
3. Cheng K, Cai N, Zhu J, Yang X, Liang H, Zhang W. Tumor-associated macrophages in liver cancer: From mechanisms to therapy. *Cancer Commun (Lond)*. 2022;**42**(11):1112-40. [PubMed ID: 36069342]. [PubMed Central ID: PMC9648394]. https://doi.org/10.1002/cac2.12345.
4. Hartley-Blossom Z, Alam M, Stone J, Iannuccilli J. Microwave Ablation in the Liver: An Update. *Surg Technol Int*. 2020;**37**:72-8. [PubMed ID: 32681731].
5. Rix A, Lederle W, Theek B, Lammers T, Moonen C, Schmitz G, et al. Advanced Ultrasound Technologies for Diagnosis and Therapy. *J Nucl Med*. 2018;**59**(5):740-6. [PubMed ID: 29496981]. https://doi.org/10.2967/jnumed.117.200030.
6. Spiliotis AE, Gabelein G, Hollander S, Scherber PR, Glanemann M, Patel B. Microwave ablation compared with radiofrequency ablation for the treatment of liver cancer: a systematic review and meta-analysis. *Radiol Oncol*. 2021;**55**(3):247-58. [PubMed ID: 34167181]. [PubMed Central ID: PMC8366737]. https://doi.org/10.2478/raon-2021-0030.
7. Mellema DC, Song P, Kinnick RR, Trzasko JD, Urban MW, Greenleaf JF, et al. Probe Oscillation Shear Wave Elastography: Initial In Vivo Results in Liver. *IEEE Trans Med Imaging*. 2018;**37**(5):1214-23. [PubMed ID: 29727284]. [PubMed Central ID: PMC5937941]. https://doi.org/10.1109/TMI.2017.2780855.
8. Fouad R, Elbaz T, Abdel Alem S, Elsharkawy A, Negm M, Khairy M, et al. Evaluation of accuracy of elastography point quantification versus other noninvasive modalities in staging of fibrosis in chronic hepatitis C virus patients. *Europ J Gastroenterol Hepatol*. 2018;**30**(8):882-7. https://doi.org/10.1097/meg.0000000000001151.
9. Chen YL, Gao Y, Chang C, Wang F, Zeng W, Chen JJ. Ultrasound shear wave elastography of breast lesions: correlation of anisotropy with clinical and histopathological findings. *Cancer Imaging*. 2018;**18**(1):11. [PubMed ID: 29622044]. [PubMed Central ID: PMC5887177]. https://doi.org/10.1186/s40644-018-0144-x.
10. Zhu H, Zhu C. An experimental study of shear wave elastography for quantitatively evaluating the injury of rabbit liver tissue after microwave thermal ablation. *Hainan Med J*. 2020;**31**(20):2585-8.
11. Yang W, Varghese T, Ziemlewicz T, Alexander M, Lubner M, Hinshaw JL, et al. Delineation of Post-Procedure Ablation Regions with Electrode Displacement Elastography with a Comparison to Acoustic Radiation Force Impulse Imaging. *Ultrasound Med Biol*. 2017;**43**(9):1953-62. [PubMed ID: 28595851]. [PubMed Central ID: PMC5523876]. https://doi.org/10.1016/j.ultrasmedbio.2017.04.021.
12. Sohn JT. Resource equation method for sample size calculation in animal studies. *Am J Emerg Med*. 2023;**63**:175-6. [PubMed ID: 36336539]. https://doi.org/10.1016/j.ajem.2022.10.041.
13. Wu Q, Na-shun B, Chen L, Gu W. Anesthetic Effect of Pentobarbital Sodium in Combination with Sumianxin Ⅱ on Tibet Mini-Pigs. *Chin J Comparative Med*. 2008;**18**(10):29-31.
14. Ferraioli G, Barr RG. Ultrasound liver elastography beyond liver fibrosis assessment. *World J Gastroenterol*. 2020;**26**(24):3413-20. [PubMed ID: 32655265]. [PubMed Central ID: PMC7327790]. https://doi.org/10.3748/wjg.v26.i24.3413.
15. Luo C, Lin J, Liu G, He G, Zuo Y, Dai L, et al. Preliminary Exploration on the Value of Shear Wave Elastography in Evaluating the Effectiveness of Microwave Ablation on Hepatic Malignancies. *Ultrasound Q*. 2022;**38**(2):160-4. [PubMed ID: 35394990]. https://doi.org/10.1097/RUQ.0000000000000606.
16. Geoghegan R, Ter Haar G, Nightingale K, Marks L, Natarajan S. Methods of monitoring thermal ablation of soft tissue tumors - A comprehensive review. *Med Phys*. 2022;**49**(2):769-91. [PubMed ID: 34965307]. https://doi.org/10.1002/mp.15439.
17. Fahey BJ, Hsu SJ, Wolf PD, Nelson RC, Trahey GE. Liver ablation guidance with acoustic radiation force impulse imaging: challenges and opportunities. *Phys Med Biol*. 2006;**51**(15):3785-808. [PubMed ID:

16861781]. [PubMed Central ID: PMC2238173]. https://doi.org/10.1088/0031-9155/51/15/013.

18. Pohlman RM, Hinshaw JL, Ziemlewicz TJ, Lubner MG, Wells SA, Lee FJ, et al. Differential Imaging of Liver Tumors before and after Microwave Ablation with Electrode Displacement Elastography. *Ultrasound Med Biol*. 2021;**47**(8):2138-56. [PubMed ID: 34011451]. [PubMed Central ID: PMC8243838]. https://doi.org/10.1016/j.ultrasmedbio.2021.03.027.
19. Gimenez ME, Davrieux CF, Saccomandi P, Serra E, Quero G, Palermo M, et al. Applications of Elastography in Ablation Therapies: An Animal Model In Vivo Study. *J Laparoendosc Adv Surg Tech A*. 2020;**30**(9):980-6. [PubMed ID: 32668183]. https://doi.org/10.1089/lap.2020.0485.
20. Crocetti L, Calcagni F, Gherarducci G, Tosoratti N, Amabile C, Tarantino FP, et al. Monitoring of Thermal-Induced Changes in Liver Stiffness During Controlled Hyperthermia and Microwave Ablation in an Ex Vivo Bovine Model Using Point Shear Wave Elastography. *Cardiovasc Intervent Radiol*. 2019;**42**(5):744-50. [PubMed ID: 30603965]. https://doi.org/10.1007/s00270-018-02152-y.
21. Luo C, Li T, Li Z, Zuo Y, He G, Lin J, et al. Evaluation of Microwave Ablation Efficacy by Strain Elastography and Shear Wave Elastography in ex Vivo Porcine Liver. *Ultrasound Med Biol*. 2021;**47**(9):2636-45. [PubMed ID: 34140168]. https://doi.org/10.1016/j.ultrasmedbio.2021.05.009.
22. Zhou H, Zhang J, Wang F, Han Z, Cheng Z, Feng L, et al. The clinical value of ultrasound elastography in evaluating uterine leiomyomas and adenomyosis treated with percutaneous microwave ablation. *Chin J Ultrasonography*. 2012:149-52.
23. Tian W, Lv J, Xie X, Lin M, Zhou L, Huang G, et al. Real-time shear wave elastography in the evaluation of radiofrequence ablation for liver tumours: a clinical study [J/CD]. *Chin J Med Ultrasound (Electronic Version)*. 2014;**11**(12).
24. Kang J, Kwon H, Cho J, Oh J, Nam K, Yoon S, et al. Comparative study of shear wave velocities using acoustic radiation force impulse technology in hepatocellular carcinoma: the extent of radiofrequency ablation. *Gut Liver*. 2012;**6**(3):362-7. [PubMed ID: 22844566]. [PubMed Central ID: PMC3404175]. https://doi.org/10.5009/gnl.2012.6.3.362.
25. Huang L, Zhang Z, Zhu C. Evaluation of the effect of microwave ablation of pork liver with supersonic shear imaging in vitro. *J Ultrasound Clin Med*. 2016;(2):73-6.
26. Zhang Z, Zhu C, Ma C. Preliminary Study of Shear Wave Elastography in Evaluating Microwave Ablation of In Vitro Pork Livers. *Chin J Med Imaging*. 2016;**24**(9):650-3.